

BI-DIRECTIONAL RESPONSE OF BASE ISOLATED STRUCTURES SUBJECTED TO NEAR-FAULT GROUND MOTIONS

S. Berton¹, J.E. Bolander² and A. Pasion¹

¹*Studio Projecta, Environmental and Structural Engineering Consulting,
via A. Bugatti 40, Jesolo, Venezia, Italy*

²*Professor, Dept. of Civil and Environmental Engineering, University of California, Davis,
One Shields Avenue, Davis, California, USA*

Email: ss.berton@tiscali.it, jebolander@ucdavis.edu, antoniopasian@libero.it

ABSTRACT :

This paper presents the results of a parametric study on the effect of near-fault ground motions on the response of base isolated structures. The isolator-structure system is modeled as a rigid mass mounted on a single isolation bearing. An analytical model based on classical rate-independent plasticity is used for representing the bidirectional coupling effect and the bilinear behavior exhibited by many of the current seismic isolation devices. A series of time history analyses is carried out using two pairs of input ground motions (N-S and W-E horizontal components) recorded during the major event of the 1999 Chi-Chi Taiwan earthquake. Both ground motions have been recorded in locations close to the generating fault but only one presents strong near-fault characteristics. In each of the analysis sets the model parameters are varied and the system responses compared. The results of this study confirm that near-fault ground motions are associated with larger isolator deformation demands. Furthermore, the results indicate that, among the three parameters that characterize the bilinear oscillator model, the isolator strength, or equivalently the yielding force, is the key parameter to reduce isolator deformations when subjected to near-fault ground motions.

KEYWORDS:

Base isolation, Seismic mitigation, Near-fault effect, Bi-linear response

1. INTRODUCTION

Ground motions recorded in the proximity of the generating fault might present peculiar characteristics due to the so-called directivity and fling effects (Kramer, 1996). The directivity effect is the result of a mutual interference of the seismic waves that sum up their effects as they travel along the fault in the direction of the propagating rupture. Fling effect results from tectonic deformation at the site and is related to the slip on the fault near the site. Both directivity and fling effects can lead to ground motions with very large peak ground velocities (PGV) and peak ground displacements (PGD), distinct long-period pulses in their records and large permanent ground displacements. Such ground motions are usually referred as near-fault or near-field ground motions. They can induce particularly large deformation demands on modern flexible structures such as high-rise buildings, long-span bridges (Hall, 1995 and Malhotra, 1999), as well as base isolated structures (Jangid, 2001). Previous studies and recent in-field observations have raised serious concerns about the safety of flexible structures located in potential near-fault regions and in particular on the effectiveness of base isolations for structures located in such areas.

Base isolators have been used in many applications for seismic protection of historical buildings and other important structures such as hospitals and nuclear power plants, but also in bridges and residential buildings (Skinner, 1993). Base isolation consists of inserting between the structure and the support system special devices called isolators that possess high lateral flexibility and high axial rigidity. The main effect is a shift of the fundamental period of the isolated structure toward higher values and toward the tail portion of the site response spectrum generally associated with smaller structural responses. Examples of isolators include sliders such as Friction Pendulum Systems (FPS), Lead Rubber Bearings (LRB) and Hysteretic Bearings (HB). FPSs are sliders that utilize spherical sliding surfaces to provide restoring capacity to the system (Zayas, 1990). LRB isolators

consist of pads of rubber compounds reinforced with a cylindrical lead core to increase the energy dissipation capacity of the isolator (Skinner, 1993). HB isolators combine the use of low-friction sliding supports with special mild steel components that are designed to deform and yield as the device is activated. An example of HB isolators is the yielding steel device (Roussis, 2003).

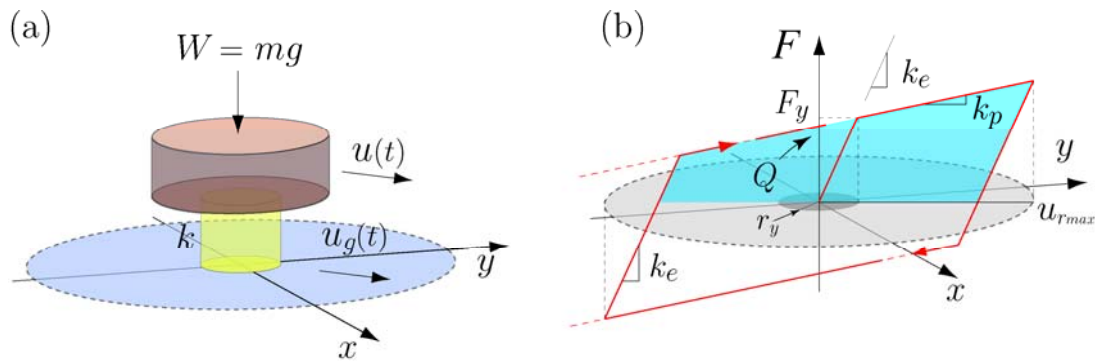


Figure 1. (a) 2-degree-of-freedom (2DOF) model of an isolation system;
 (b) bilinear force-displacement loop.

Previous studies have shown that the response of an isolated system subjected to bidirectional seismic excitation differs significantly from those considering only one horizontal component of the ground motion (Warn, 2004). In this paper, the effect of near-fault ground motions on base isolation systems is investigated numerically. The isolation system is represented as a rigid mass mounted on a single isolator which is modeled by a bi-directional rate-independent coupled plasticity model. Most of the currently available isolators present a force-displacement response that can be approximated by a bilinear relation (Makris, 2004). The three independent parameters used in this study to characterize the isolator bilinear response are the unidirectional yielding force, the yielding displacement and the post-yielding period. The nonlinear time history analysis series are carried out using two input ground acceleration pairs (N-S and W-E components) recorded during the 1999 Chi-Chi Taiwan earthquake. Although these two pairs of data have been recorded during the same event at locations that are close to each other and very close to the generating fault, only one pair presents distinct near-fault characteristics with a pulse-like velocity record, and a high PGV/PGA ratio. The approach used in this study consists of varying the three independent parameters within selected practical limits for different type of isolators. The results are then compared and the influence of each parameter on the isolation displacement demand and on the isolation capacity of the system is presented and discussed.

2. MODELING

Figure 1a shows a schematic representation of the 2 degree-of-freedom (2DOF) bilinear oscillator model. The model can be a simple representation of a single-span concrete deck bridge with isolators on each abutment or an isolated rigid building with regular shape and mass distribution. The isolator response is modeled using a rate-independent coupled plasticity model with linear kinematic hardening (Simo, 1998) that may be considered a bidirectional generalization of a bilinear unidirectional model. The model is based on the assumption of isotropic behavior in x and y directions and neglects torsion of the bearing. The restoring force of the bearing $F = [F_x \ F_y]^T$ is assumed to depend only on the translational deformation of the bearing $U = [u_x \ u_y]^T$. In this model a circular isotropic yield function f is postulated:

$$f = \| F - \alpha_y \| - r_y \quad (2.1)$$

where α_y is the internal variable called the “back force” and r_y is the radius of the yielding surface in displacement space. Within this yield surface the response is linear isotropic with the force related to the displacement by a constant stiffness parameter k_e (Fig. 1b). In combination with the elastic-plastic decomposition of the displacement vector $U = U^e + U^p$ where U^e is the elastic recoverable deformation and U^p the plastic component, the isolator force

can be written as:

$$F = k_e U^e = k_e (U - U^p) \quad (2.2)$$

An associated flow rule is introduced which implies that the evolution of the plastic displacement vector is always normal to the yielding surface in force space such that:

$$\dot{U}^p = \dot{\gamma} \cdot n \quad (2.3)$$

where n is the normal to the yielding surface and $\dot{\gamma}$ is the consistency parameter. The consistency parameter must satisfy the Kuhn-Tucker conditions. In addition a linear kinematic hardening rule is specified, with:

$$\dot{\alpha}_y = k_h \cdot \dot{U}^p \quad (2.4)$$

where k_h is a constant hardening modulus. The system deformation is determined in a discrete time regime by solving the equation of motion:

$$M\ddot{U} + C\dot{U} + k_e(U - U^p) = -M\ddot{U}_g \quad (2.5)$$

where M and C are the 2x2 mass and damping matrices respectively, \ddot{U}_g is the input ground acceleration vector and $k_e(U - U^p)$ is the isolator force. A return mapping algorithm (Simo, 1998) is used to determine the evolution of U^p over each time step. The solution U is obtained by numerically integrating the incremental form of the equation of motion of Eq. 2.5 using standard procedures. A damping ratio $\xi=4\%$ is used for all the numerical analyses presented in this study.

Table 1 Ground motion data from the 1999 Chi-Chi Taiwan earthquake.

Recording Station / comp.	Fault rupture dist. (km)	¹ Soil type	PGA (g)	PGV (cm/s)	PGD (cm)	PGV/PGA (cm/s)
TCU129 N-S	1.18	C	0.634	36.1	28.87	56.94
TCU129 E-W	1.18	C	1.010	60.00	50.15	59.40
TCU068 N-S	0.33	C	0.462	263.10	430.00	569.48
TCU068 E-W	0.33	C	0.566	176.60	324.11	312.01

¹USGS soil classification

3. INPUT GROUND MOTIONS

Two pairs of ground motions recorded during the magnitude 7.6, 1999 Chi-Chi Taiwan earthquake are used to carry out all the nonlinear time history analyses presented in this paper. Table 1 shows the most significant parameters that characterize the two pairs of ground motions. The TCU129 receiving station is located on the footwall side of the 1999 Chi-Chi earthquake-generating fault (i.e. on the west side of the observed surface fracture) and, despite its vicinity to the fault rupture and epicenter (1.18 and 11.9 km, respectively), the records do not present near-fault pulse-type characteristics. The peak ground accelerations (*PGA*) of these records are very high, while the peak ground velocities (*PGV*) and displacements (*PGD*) are only moderately high. The TCU068 receiving station was located on the hanging wall of the fault, just 0.33 km southeast of the observed surface fracture. In contrast, the TCU068 records present strong near-fault pulse-like characteristics emphasized by the large *PGV* and *PGD*, and by the high values of the ratio *PGV/PGA*. The data of both records and the information

listed in Table 1 have been obtained from the PEER Strong Ground Motion database (<http://peer.berkeley.edu/smcat>).

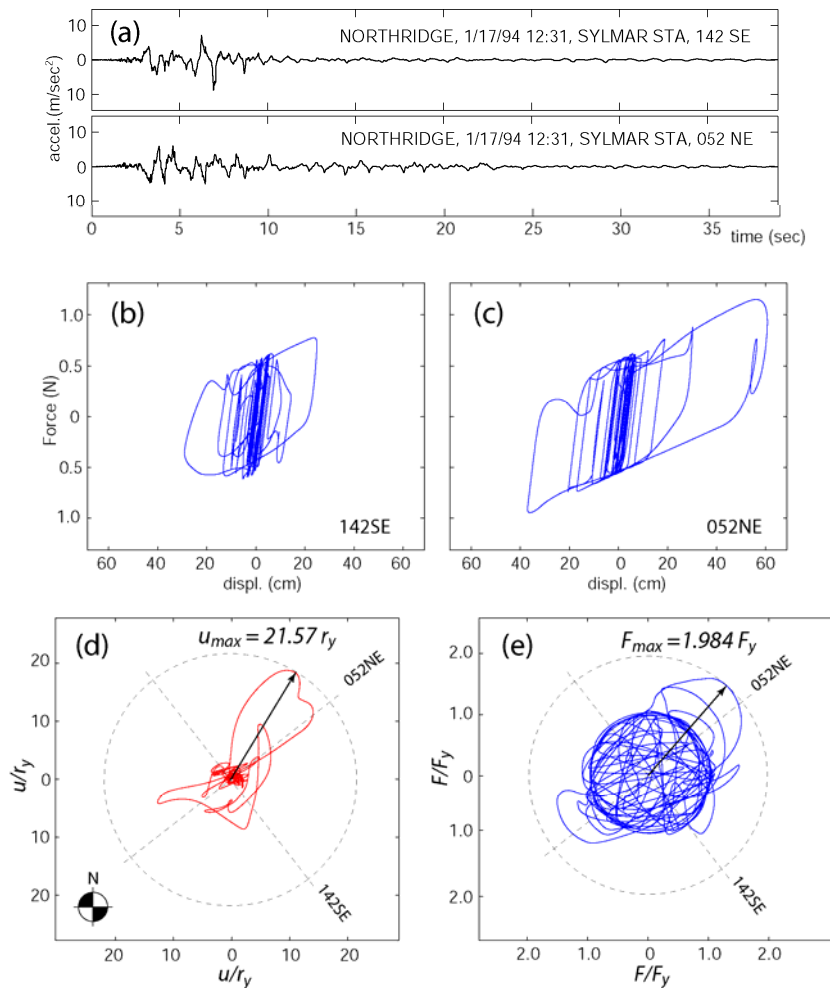


Figure 2. (a) Northridge Earthquake input ground accelerations; (b) and (c) model force-displacement responses; (d) normalized displacement path response, and (e) normalized force path response of the model.

4. PARAMETER RANGES SELECTION

The 2DOF bilinear oscillator model, schematically shown in Fig. 1a, is used to characterize the response of an isolated structure. Besides the system mass m , three more parameters are necessary to characterize the nonlinear response of the model. The three parameters selected are the yielding or plastic force F_p (radius of the yielding surface in force space), the yielding displacement r_y (radius of the yielding surface in displacement space) and the post-yield period T_p . The plastic force F_p is used for convenience instead of the system strength Q , where the relation between these two parameters can be written as $Q = (1 - \alpha)F_p$, in which α is the ratio between the post-yield and the initial elastic stiffness (Fig. 1b). In addition, the yielding force F_p is selected as a fraction of the tributary weight $W = mg$ supported by the isolator. Because of this, the numerical results become completely independent on the system mass. Typical values of yielding force for civil engineering applications range between 3 to 15% of W . In this study five values of the ratio $\gamma = F_p / W$ are selected: $\gamma = 0.03, 0.06, 0.09, 0.12$ and 0.15 . Three values of the yielding radius r_y are used in this study: $r_y = 0.5, 15$ and 50 mm. The value of $r_y = 0.5$ mm represents sliders such as FPS devices whose elastic limit deformations of the bearing components in the no-slip conditions are small ranging from 0.2 to 0.5 mm (Makris, 2004). The other two values of r_y were selected to

represent LRB and HB that usually present yielding deformations that can vary between one to several centimeters (Skinner, 1993; Roussis, 2003). The period T_p calculated from the post-yield stiffness (i.e. $T_p = 2\pi\sqrt{m/k_p}$) is used as the third independent parameter that characterizes the isolator bilinear response. The post-yield period T_p , often referred as the isolator period, is an important parameter traditionally associated with the isolator ability to self-center (Berton, 2007). Typical values of T_p are in the range of a few seconds (e.g. 3-5 s). In this study 14 values of T_p distributed within the two selected practical limits of $T_p=2.0$ s and 10.0 s are used.

5. PARAMETRIC STUDY APPROACH

The model performance is evaluated in terms of peak deformation of the isolator and peak acceleration felt by the isolated mass. Figure 2 shows an example of analysis outputs in which the model having a 30 mm yielding radius, post-yield period of 6 s, and yield force equal to 6% of the tributary weight W , is subjected to the two horizontal components of the 1994 Northridge earthquake recorded at the Sylmar station. Figure 2a shows the ground acceleration records of the 6.7 magnitude seismic event. The *PGA* of the 052NE component is 0.612 g while for the 142SE component is 0.897 g. Figures 2b and 2c show the plots of the corresponding force-displacement loops. The full displacement and force-normalized paths are shown in Figs. 2d and 2e, respectively. The maximum displacement vector and maximum force vector recorded during the simulation are also shown in these two figures. The maximum displacement occurs at time $t=3.81$ s and its value is 64.7 cm ($21.57 r_y$). The maximum value of the computed force occurs at the computational time $t=3.70$ s and its value is 1.984 times the yield force F_p . Both the displacement and force peak values are recorded and used for the parametric analysis.

6. ANALYSIS RESULTS

The analysis results for the two motions without and with near-fault characteristics are summarized in Figs. 3 and 4, respectively. For each of the three values of yielding displacement and for each input ground motion, the selected fourteen values of post-yield periods and the five values of yielding force result in 70 combinations (i.e. 70 different analyses). The three plots in the left column of each figure, one for each choice of yielding radius, r_y , show the model peak deformations (*MPD*). Similarly, the three plots in the right column represent the model peak accelerations (*MPA*). The *MPD* and *MPA* values are portrayed as three-dimensional function of the two independent variables, the ratio γ (i.e. F_p/W) and the post-yield period T_p .

Figure 3 summarizes the results of the analyses carried out using the TCU129 records. Despite the high value of *PGA* (1.192 g combining the two components), these records do not present near-fault pulse-like characteristics. The three plots on the left of the figure show the peak displacements (*MPD*) for each of the three selected values of the radius r_y . The *MPD* values range from a minimum of 120 mm recorded for the case $r_y=15$ mm, $\gamma=12\%$ and $T_p=2$ s, and a maximum of 792 mm for the case $r_y=0.5$ mm, $\gamma=3\%$ and $T_p=10$ s. Similarly, the three plots on the right of the Fig. 3 represent the peak acceleration values provided by the numerical analyses for the selected ranges of T_p and γ and for the three value of r_y . The *MPA* values range from a minimum of 0.046 g recorded for the case $r_y=50$ mm, $\gamma=3\%$ and $T_p=10$ s, and a maximum of 0.366 g for the case $r_y=0.5$ mm, $\gamma=12\%$ and $T_p=2$ s. The maximum value of 0.366 g obtained from the analysis is much lower than the *PGA*. In terms of *MPD*, although the peak values are moderately high, especially for the analysis cases corresponding to $r_y=0.5$ mm, in general they are within the deformation capacity of the currently used isolation devices. Therefore we can conclude that within the ranges of parameters selected for this study, base isolation is quite effective for this particular ground motion.

Figure 4 shows the results of the analysis for the TCU068 records. As mentioned in section 3, this station was located in an area within the forward directivity region of the main shock of the Chi-Chi earthquake and therefore the records present strong near-fault pulse-like characteristics. The three plots of the peak displacements values are shown in the right side of the Fig. 4. Although their trends are similar to the corresponding plots of Fig.3 (note that different scale factors are used) the peak values are significantly higher ranging from a minimum of 258 mm recorded for the case

$r_y=0.5$ mm, $\gamma=15\%$ and $T_p=2$ s, and a maximum of 4925 mm for the case $r_y=50$ mm, $\gamma=3\%$ and $T_p=10$ s. This maximum value is clearly above the maximum displacement capacity of regular isolators. The differences between the *MPD* values for the TCU129 and TCU068 records are around one order of magnitude for the cases $r_y=15$ and $r_y=50$ mm while the results indicate that the *MPDs* of the TCU068 for the case $r_y=0.5$ mm are only about 2.5 times of the *MPDs* of the TCU129 records. The three plots on the right side of Fig. 4 show the *MPA* results. Similar to the TCU129 ground motion, the maximum values of the *MPAs* always have maximum that occur for smaller post-yield periods and then decrease rapidly toward their minimum values at $T_p=10$ s. For these records, the minimum value of 0.091 g is obtained from the analysis case with $u_y=0.5$ mm, $T_p=10$ s and $\gamma=3\%$, while the maximum of 0.827 g corresponds to the case with $u_y=50$ mm, $T_p=2$ s and $\gamma=3\%$. Some points of the *MPA* surfaces exceed the PGA value (0.806 g), denoting that some combinations of T_p and γ correspond to models that instead of isolating the mass amplify the effect of the ground motion.

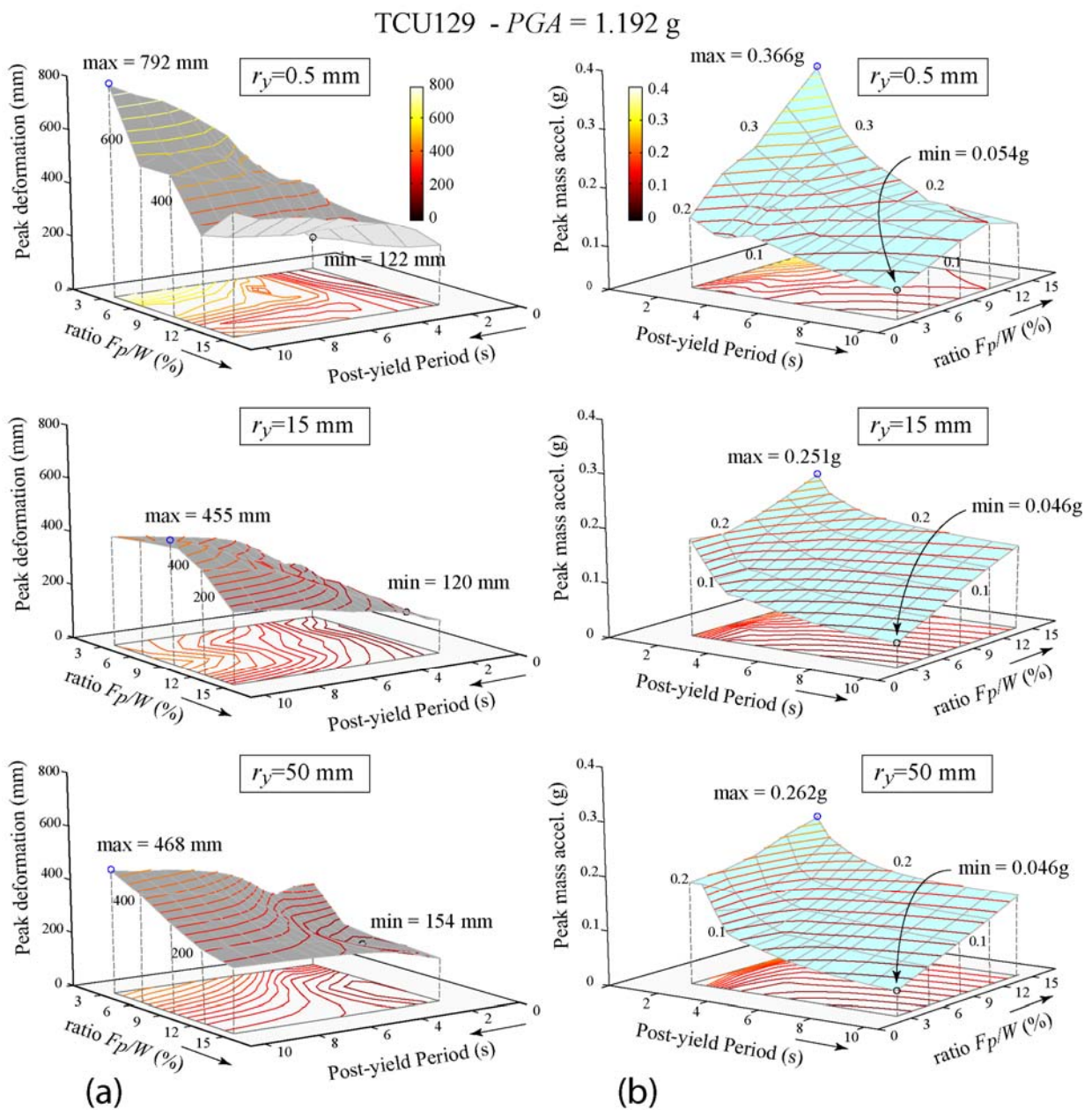


Figure 3. Analysis results for the TCU129 Chi-Chi Taiwan earthquake;
 (a) model peak deformations; (b) model peak mass accelerations.

By observing the analysis results shown in Figs 3 and 4 some general trends can be observed. The minimum values of *MPD* (best performance in terms of deformations) always occur for high values of yielding force ($\gamma=12\%$ and $\gamma=15\%$) and in general for small values of isolator period ($T_p=2$ s); the minimum of *MPA* (best performance in terms of mass isolation) occur for small values of γ ($\gamma=3\%$, 6%) and for high values of T_p ($T_p=10$ s). In addition, if we keep T_p constant and for high values of T_p , the isolation capacity of the system in terms of acceleration transmitted to the mass does not change significantly as γ increases from 0.3 to 1.5. This is particularly true for the TCU068 analysis cases. Therefore, it can be concluded that for the cases analyzed, parameter combinations with high value of γ and high value of T_p not only result in minimum isolator deformations but also provide sufficiently good isolation to the system mass.

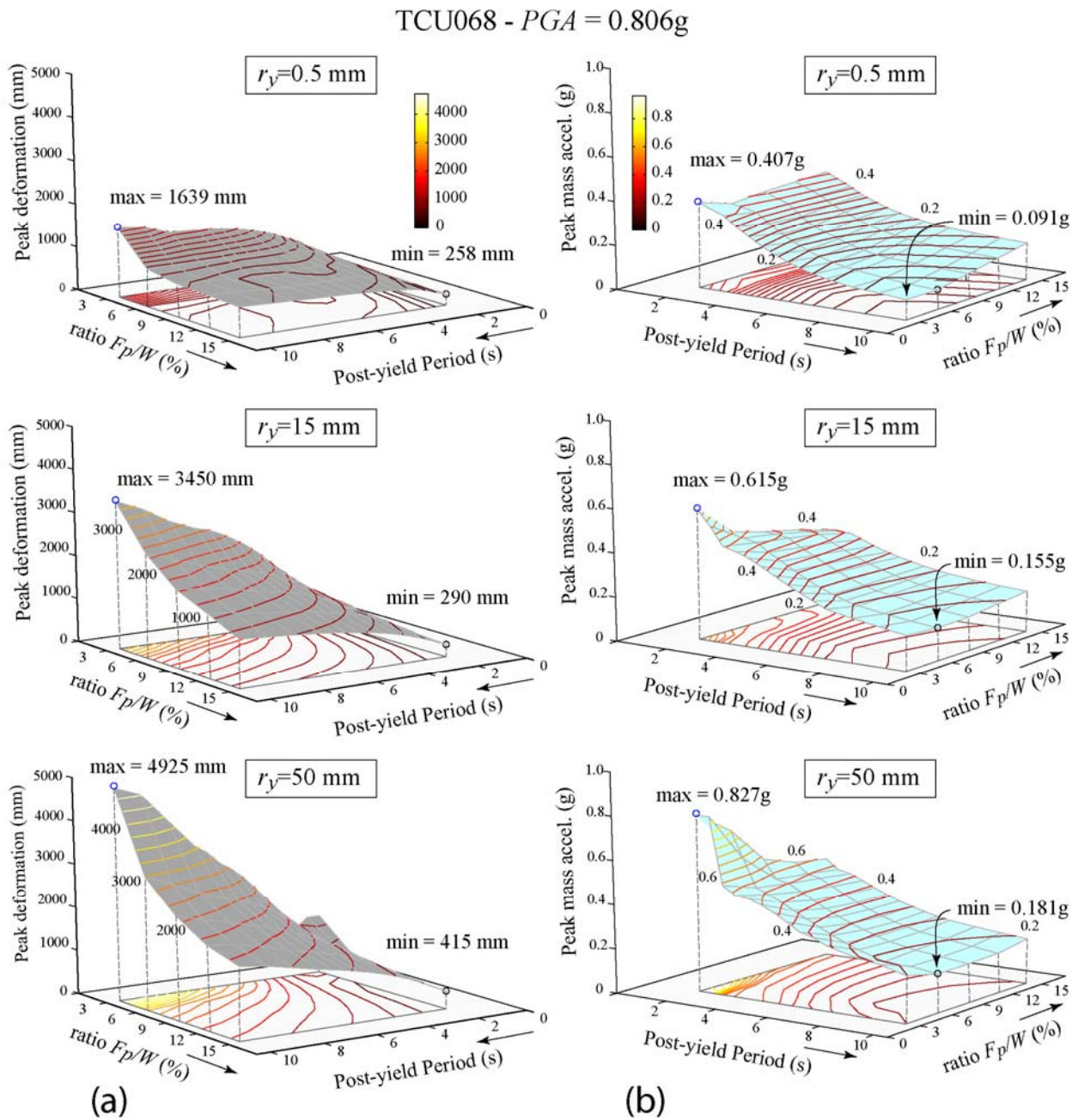


Figure 4. Analysis results for the TCU068 Chi-Chi Taiwan earthquake; (a) model peak deformations; (b) model peak mass accelerations.

7. CONCLUSIONS

This paper presents the results of a parametric study based on a set of numerical simulations of simple base isolation system models. The main goal is to provide information on the influence of each of the parameters that characterize the model on the system response when subjected to ground motions having near-fault pulse-like characteristics. From the analysis results the following conclusions can be drawn

- The case analyzed in this paper confirm that near-fault ground motions having pulse-like characteristics can induce unusually large deformations on flexible structures such as base isolated structures;
- The yielding radius r_y appears to have a significant influence on the peak deformation response of the system. Nevertheless, it is likely that the fictitious value of the damping ratio $\xi = 4\%$ set for all the analyses might have a strong influence on the system response for small values of yielding radius. Further studies on this particular aspect need to be done.
- The high value of the yielding force (i.e. $\gamma = 15\%$) combined with high values of the post-yield period (5-10 s) is the best parameter combination to achieve both smaller device deformations and good isolation in terms of acceleration transmitted to the isolated structure when the system is subjected to near-fault ground motions. This result is partially in contradiction with the common believe that high values of post-yield periods, that is usually associated with poor re-centering capacity of the system, imply also large device deformations. This study indicates that the yielding-force is the key parameter to control the peak deformation of an isolation system when subjected to near fault ground motions.

REFERENCES

- Berton, S., S. Infanti, M. G. Castellano and H. Hikosaka (2007). Self-centering capacity of seismic isolation systems. *Journal of Structural Control and Health Monitoring* **14:6**, 895-914.
- Hall, J.F., T. H. Heaton, M. W. Halling and D. J. Wald (1995). Near-source ground motion and its effects on flexible buildings. *Earthquake Spectra* **11:4**, 569-605.
- Jangid, R. S. and J. M. Kelly (2001). Base isolation for near-fault ground motion. *Earthquake Engineering and Structural Dynamics* **30**, 691-707.
- Kramer, S. L. (1996). Geotechnical Earthquake Engineering, Prentice Hall, Upper Saddle River, New Jersey.
- Malhotra, P. K. (1999). Response of buildings to near-field pulse-like ground motions. *Earthquake Engineering and Structural Dynamics* **28**, 1309-1326.
- Makris N. and C. J. Black (2004). Dimensional analysis of bilinear oscillators under pulse-type excitations. *Journal of Engineering Mechanics (ASCE)* **130:9**, 1019-1031.
- Simo, J. C. and T.J.R. Hughes (1998). Computational Inelasticity, Springer Science+Business Media LCC, New York, NY.
- Roussis P.C., M.C. Constantinou, M. Erdik, E. Durukal and M. Dicleli (2003). Assessment of performance of seismic isolation system of Bolu viaduct. *Journal of Bridge Engineering (ASCE)* **8:4**, 182-190.
- Skinner R. I., W. H. Robinson and G.H. Mc Verry (1993). An introduction to seismic isolation. John Wiley & Sons, New York.
- Warn G. P and A.S. Whittaker (2004). Performance estimates in seismically isolated bridge structures. *Engineering Structures* **26**, 1261-1278.
- Zayas V. A., S. S. Low and S. A. Mahin (1990). A simple pendulum technique for achieving seismic isolation. *Earthquake Spectra* **6:2**, 317-333.